Article

Journal of
Nanoscience and Nanotechnology
Vol. 15, 7181–7185, 2015
www.aspbs.com/jnn

Self-Assembled Microspheres Formed from α-MnO_2 Nanotubes as an Anode Material for Rechargeable Lithium-Ion Batteries

S. Savut Jan[1, 2], S. Nurgul[3], Xiaoqin Shi[1], and Hui Xia[1, 2, *]

[1] School of Materials Science and Engineering, Nanjing University of Science and Technology, Nanjing 210094, China
[2] Herbert Gleiter Institute of Nanoscience, Nanjing University of Science and Technology, Nanjing 210094, China
[3] Department of Physics and Institute of Biophysics, Central China Normal University, Wuhan 430079, China

Self-assembled microspheres formed from single-crystal α-MnO_2 nanotubes have been successfully synthesized by a facile hydrothermal treatment of $KMnO_4$ in the hydrochloric acid solution. The effect of the reaction time on the microstructure and morphology of the sample is investigated systemically. Meanwhile, the forming mechanism of nano-structured α-MnO_2 is carefully studied by X-ray powder diffraction, field emission scanning electron microscopy, transmission electron microscopy and high-resolution transmission electron microscopy. The MnO_2 nanotube microspheres exhibit large reversible capacity up to 807 mA h g^{-1} as well as good cycling stability and rate capability, making them promising as anode material for lithium-ion batteries.

Keywords: α-MnO_2 Nanotube, Hydrothermal Treatment, Nanoflake.

1. INTRODUCTION

A nanoscale approach to electrochemical energy storage applications such as in the lithium ion batteries and supercapacitors has been of great interest owing to their unique properties leading to improved performance.[1–5] Innovative materials chemistry has been the key to various advancements in lithium rechargeable batteries.[6, 7] In recent years, various transition metal oxides have been extensively studied as electrode materials for lithium ion batteries because of their high theoretical capacity, safety, environmental benignity, and low cost.[8–15] Among the transition metal oxides, manganese dioxide (MnO_2) has been widely studied as both anode and cathode for lithium ion batteries with a high storage capacity. It was reported that MnO_2 has dissimilar kinds of polymorphs, such as α-, β-, γ- and δ-MnO_2 type according to different linkage ways of its basic MnO_6 octahedral unites, and it has wide applications such as redox catalysts,[16] molecular/ion sieves[17] and electrode materials in batteries or capacitors.[18–21] Recently, growing interest has been focused on the fabrication of one-dimensional (1-D) MnO_2 nanostructures. α-MnO_2 nanorods/nanowires,[22–24] β-MnO_2 nanorods/nanotubes,[25, 26] γ-MnO_2 nanowires/nanotubes[27–29] and δ-MnO_2 nanofibers[30] have been successfully prepared by oxidation of Mn^{2+} or reduction of $KMnO_4$. In addition, single-crystal MnO_2 nanowires of α, β and γ type have also been conveniently prepared by simple hydrothermal treatment of commercial γ-MnO_2 particles in water or ammonia solution.[31, 32] It is discovered that these 1-D MnO_2 nanomaterials show excellent electrochemical properties than their bulk counterparts which can be adopted as promising electrode materials in Li–MnO_2 cells, electrochemical capacitors, and etc.[28, 33]

In this work, we report the synthesis of α-MnO_2 microspheres self-assembled from single crystal nanotubes by a direct hydrothermal approach that allows us to careful control over the crystal structure and morphology of MnO_2 nanostructures. Specially, simply changing the reaction time in our hydrothermal process, enables synthesis of three different MnO_2 nanostructures (nanoflake/nanorod and nanotube) with controlled crystal phases and morphologies. The formation mechanisms for each of these products were also studied systemically and galvanostatic charge/discharge tests for α-MnO_2 nanotubes were operated by a Newer battery system. The results show that the as-prepared α-MnO_2 nanotube microspheres display high

*Author to whom correspondence should be addressed.

reversible capacity, good cycling stability and good rate capability as anode material for lithium ion batteries.

2. EXPERIMENTAL DETAILS

All chemical reagents are of analytical grade from Aldrich. In a typical experimental procedure, 0.25 g $KMnO_4$, 0.048 g $Fe_2(SO_4)_3$ and 8 mmol concentrated H_2SO_4 were added to 80 mL deionized water under magnetic stirring to form the precursor solution. After stirring for about 15 min, the solution was transferred into a Teflon-lined stainless steel autoclave with a capacity of 100 mL. The autoclaves were then heated in an electric oven at a temperature of 150 °C for different reaction times of 1 h, 5 h, and 18 h, respectively. After the autoclave was cooled down naturally to room temperature, brown precipitate was collected by centrifugation and dried in a vacuum oven before characterization.

Crystallographic information of all as-prepared samples were investigated with X-ray powder diffraction (XRD, Shimadzu XRD-6000, Cu Kα, $\lambda = 1.5406$ Å) at a scanning rate of 1 °C min^{-1}. The morphology of as-prepared samples were examined with field-emission scanning electron microscopy (FESEM, JSM-6700 F) and Transmission electron microscopy (TEM) and high-resolution transmission electron microscopy (HRTEM, Philips FEG CM300, 300 KV).

To investigate the electrochemical behavior, the as-prepared samples were assembled into Swagelok cells in an argon-filled glove box with moisture and oxygen below 1 ppm. The working electrode was prepared by mixing 80 wt% of the active material, 10 wt% carbon black and 10 wt% polyvinylidene difluoride (PVDF) dissolved in *N*-methylpyrrolidone (NMP). The slurry was pasted on the Ti foil and dried in a vacuum oven for 12 h. The loading of working electrode is typically in the range of 0.3–0.4 mg (~2 mg cm^{-2}). Li foil was used as both counter and reference electrodes. 1 M $LiPF_6$ in ethylene carbonate and diethyl carbonate (EC/DEC, v/v = 1:1) solution was used as the electrolyte. Galvanostatic charge and discharge measurements were carried out in the voltage range between 3.0 and 0.01 V at different current densities using the Newer battery system.

3. RESULTS AND DISCUSSION

The phase purity and crystal structure of the as-prepared MnO_2 samples were examined by XRD. Figure 1 shows the XRD patterns of the samples hydrothermally prepared at 150 °C for the different durations of 1 h, 5 h, and 18 h, respectively. As shown in Figure 1(a) the sample prepared for 1 h can be indexed to the pure layered birnessite-type MnO_2 (JCPDS No. 80-1098). Layered birnessite-type MnO_2, also denoted as δ-MnO_2 in the literature, has a two-dimensional (2-D) lamellar structure with an interlayer distance of 0.73 nm.[34] When the reaction time is increased

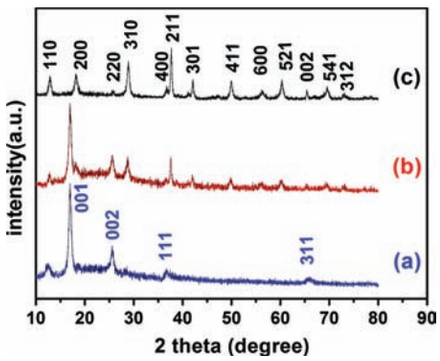

Figure 1. XRD patterns of the MnO_2 products obtained after different hydrothermal durations: (a) 1 h, (b) 5 h, and (c) 18 h.

to 5 h, the diffraction peaks of the product can be indexed to a mixture of layered birnessite-type MnO_2 and α-MnO_2 phases. All the diffraction peaks from α-MnO_2 are very weak and broad, indicating the beginning forming of the α-MnO_2 phase as the reaction time is prolonged. As the duration time increases to 18 h, all diffraction peaks of the sample can be indexed to the α-MnO_2 (JCPDS No. 44-0141) with no trace of layered MnO_2 phase. Therefore, by changing the reaction time, the phase and composition of the hydrothermally synthesized MnO_2 products can be well controlled.

The morphologies of the MnO_2 products obtained through the different hydrothermal treatments were investigated by FESEM. Figure 2(a) shows a panoramic image of the product prepared for 1 h, revealing the sample is composed of uniform microspheres with high quantity. High magnification FESEM images in Figures 2(b) and (c) indicate that this product has a microsphere/nanoflake hierarchical architecture, in which the nanoflakes are self-assembled from the center of the microspheres. Based on the previous studies, the formation mechanism of the microsphere/nanoflake hierarchical architecture could be elucidated as follows.[35–37] At the initial stage, the high concentrations of precursor lead to rapid formation of a large number nuclei in a short duration, and these nuclei self-assemble to form nearly amorphous spheres. Afterward, the heterogeneous growth of 2-D nanoflakes on the surface of the core is determined by the intrinsic layered crystal structure of birnessite MnO_2 and should follow a general Ostald ripening process. Figures 2(d)–(f) show the FESEM images of the product with a increased reaction time of 5 h. Figure 2(d) shows that these MnO_2 microspheres look like some natural sea urchins, with a diameter of 1–3 μm and numerous nanorods compactly growing around their surfaces. As shown in Figures 2(e) and (f), the as-prepared nanorods, typically 1–2 μm in length, have a square cross-section with an edge length in the range of 40–80 nm. After 18 h of hydrothermal treatment, the FESEM image of the synthesized sample (Fig. 2(g)) reveals that the final product becomes an interesting hollow microsphere structure with cavities being clearly observed. As shown in

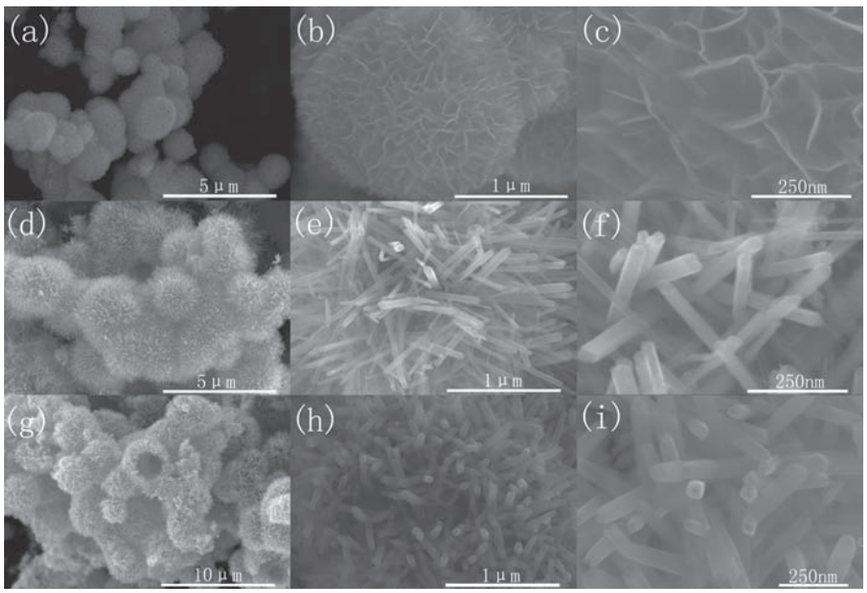

Figure 2. FESEM images of samples prepared after different hydrothermal durations: (a)–(c) 1 h, (d)–(f) 5 h, and (g)–(i) 18 h.

high magnification FESEM images of Figures 2(i) and (h), based on the above observation, the formation mechanism of these nanorods and nanotubes is explained as follows: initially, $KMnO_4$ is gradually decomposed into MnO_2 and O_2 under an acidic solution and a high pressure of hydrothermal envirment, resulting in a large quantity of MnO_2 colloids. Meanwhile, minor colloids might grow into a few small nanorods because of their relatively high concentration and surface energies under the specific experimental condition. Consequently, the reaction rate would be slowed down when the $KMnO_4$ was decomposed completely and then the whole system would keep the thermodynamically stable state. Afterward, the amorpous and poorly crystalline particles in the solution would recrystallize and grow into nanorods again. The nanorods formation machinasim comply with the famous "Ostard ripening process" in which the high quantity of nanorods are formed due to the anistropic growth driven by the chemical potential under hydrothermal condition. Finally, the formed nanorods were transformed into the hollowed nanotubes due to the chemical etching process.[38, 39] The FESEM results confirmed that the presence of Fe^{3+} ions in the hydrothermal solution plays a critical part in the formation of α-MnO_2 nanotubes when the reaction time was prolonged for 18 h. It was reported that the molar ratio between $KMnO_4$ and $Fe_2(SO_4)_3$ is a principal factor for the formation of α-MnO_2 nanotubes and self-assembly.[40]

To investigate the tubular structure of the products, the 18 h sample was further investigated by TEM and HRTEM. As shown in Figure 3(a), it can be seen that the diameters of the nanotubes are in the range between 25 and 40 nm and is very uniform along the individual nanotube. A high magnification TEM image in Figure 3(b) shows that the one-dimensional nanostructure has opened end with the inner diameter of about 10–20 nm. The representative tubular structure of the product confirms the formation of the nanotubes. Figure 3(c) shows the selected area electron diffraction pattern taken from a single α-MnO_2 nanotube, revealing the single crystalline feature of the nanotube. A HRTEM image of the as-prepared α-MnO_2 nanotube is presented in Figure 3(d), where the lattice fringes with spacing of 0.25 nm can be clearly observed, corresponding to the (400) planes of

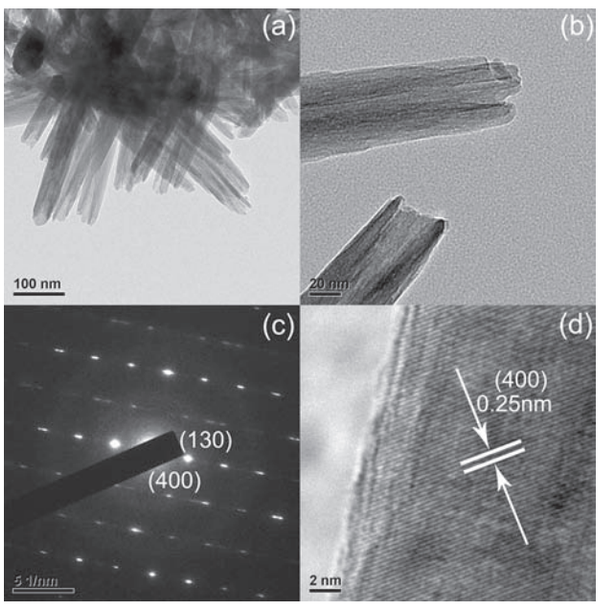

Figure 3. TEM (a) and (b) images of the sample obtained by 18 h hydrothermal treatment. SAED pattern (c) and HRTEM (d) of a individual α-MnO_2 nanotube.

the tetragonal α-MnO_2. Generally, the TEM and HRTEM analysis confirm the high-quality single-crystal nature of the as-prepared α-MnO_2 nanotubes.

Nanostructured transition-metal oxides, such as NiO, CuO, and CoO, as suggested by Poizot et al.,[41] can be used as anode materials for lithium-ion batteries with high reversible capacity than that of the traditional graphite. Encouraged by this idea, the electrochemical performance of the obtained α-MnO_2 nanotube microspheres was evaluated as anode material for lithium-ion batteries by galvanostatic charge–discharge measurements (Fig. 4). The charge/discharge curves at 1st, 10th, 20th, 40th, and 80th cycles for the α-MnO_2 nanotube microsphere electrode cycled between 0.01 and 3.0 V at a current density of 250 mA g^{-1} are shown in Figure 4(a). The first discharge and charge capacities of the MnO_2 nanotube microsphere electrode are 1212 and 807 mA h g^{-1}, respectively, with a coulombic efficiency of about 67%. This value is relatively higher compared to those reported in the previous literatures. The reported values for micro-sized MnO_2 are in the range of 500 to 900 mA h/g with a lower coulombic efficiency.[42, 43] It also can be seen from the the Figure 4(a) that a flat potential platea was observed at about 0.4 V,

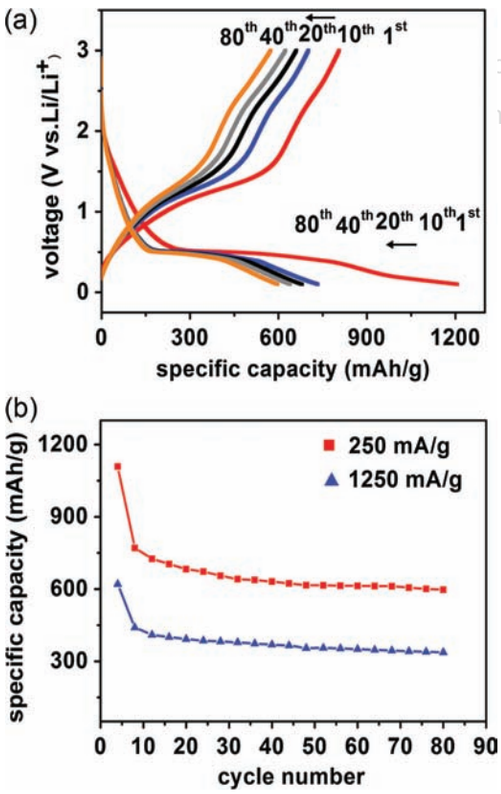

Figure 4. (a) Charge/discharge curves of as-prepared α-MnO_2 nanotube microsphere electrode at the 1st, 10th, 20th, 40th, and 80th cycles between 0.01 and 3.0 V at a current density of 250 mA h g^{-1}. (b) Cycle performance of the α-MnO_2 nanotube microsphere electrode at different current densities.

corresponding to the reduction of MnO_2 by lithium ions, the reaction between MnO_2 and Li can be described as follow:[42, 44]

$$MnO_2 + 4Li^+ + 4e^- \leftrightarrow 2Li_2O + Mn \quad (1)$$

The reaction mechanism for the transition metal oxide with lithium has been reported by Poizot et al.,[41] it is worth to notice that the formed lithium oxide is electrochemically inactive, which suggests that the extraction of lithium from lithium oxide is thermodynamically impossible. However, it has been proposed that it is possible to extract the lithium from lithium oxide with the use of nanosized materials having small particle size and unique architectural structure.[10, 45] The bulk MnO_2 exhibited a poor capacity of 120 mA h/g, but after transformed the particle size into nanoscale, it delivered a capacity higher than 800 mA h/g.[45, 46] therefore, the high reversible capacity of MnO_2 nanotubes in this work can be attributed to the nanoscale MnO_2 with distinctive hierarchical morphology which shortens the electron and lithium ion diffusion distance and expose large amount manganese atoms to the electrolyte. Besides the large reversible capacity, the MnO_2 nanotube microsphere electrode also exhibit good cycling stability with 72% of the initial reversible capacity maintained after 80 cycles. Figure 4(b) shows the cycle performance of the MnO_2 nanotube microsphere electrode at different current densities of 250 and 1250 mA g^{-1}, respectively. Even at a high current density of 1250 mA g^{-1}, the MnO_2 nanotube microsphere electrode can still deliver an initial reversible capacity of 601 mA h g^{-1}. The MnO_2 nanotube microsphere electrode also exhibits good cycling stability at the high charge discharge rate, and can deliver a reversible capacity of about 347 mA h g^{-1} after 80 cycles, which is similar to the theoretical capacity of commercial graphite (372 mA h g^{-1}).

The large reversible capacity, good cycling stability and rate capability of the MnO_2 nanotube microsphere electrode can be attributed to its unique hierarchical architecture. First, the hollowed microspheres self-assembled from the MnO_2 nanotubes provides open channels for electrolyte penetration, thus enabling large contact area between the electrode and the electrolyte. Second, the hollowed structure for the microspheres and nanotubes provides extra space to accommodate the large volume change during the Li insertion/extraction and reduce the associated strain. Finally, the small size of the nanotubes provide short diffusion paths for both lithium ions and electrons, thus favoring fast charge transport during the charge/discharge processes. With respect to the facile preparation and high yield of the products, the present α-MnO_2 nanotube microspheres represent a promising anode material for in the next-generation high performance lithium-ion batteries.

4. CONCLUSION

A facile time-dependent hydrothermal route was developed to synthesize various MnO_2 nanostructures without templates or surfactants in the reaction system. By controlling the reaction time, α-MnO_2 microspheres self-assembled from single crystalline nanotubes of 25–40 nm in diameter have been successfully prepared. The MnO_2 nanobute microsphere electrode exhibits a large reversible capacity up to 807 mA h g^{-1} as well as good cycling stability and rate capability. The superior electrochemical performance of the MnO_2 nanotube microsphere electrode can be attribute to it unique hierarchical architecture, which could accommodate large volume change and favor fast charge transport during Li insertion/extraction.

Acknowledgments: This work was supported by National Natural Science Foundation of China (No. 51102134), Natural Science Foundation of Jiangsu Province (Nos. BK20131349 and BK2011709), China Postdoctoral Science Foundation (No. 2013M530258), and Jiangsu Planned Projects for Postdoctoral Research Funds (No. 1202001B).

References and Notes

1. A. S. Arico, P. Scrosati, J. M. Tarascom, and W. Van Schalkwijik, *Nat. Mater.* 4, 366 (**2005**).
2. V. L. Pushparaj, M. M. Shaijumon, A. Kumar, S. Murugesan, L. Ci, R. Vajtai, J. R. Linhardt, O. Nalamasu, and M. P. Ajayan, *Proc. Natl. Acad. Sci. U.S.A.* 104, 13574 (**2007**).
3. J. Feng, B. Song, M. O. Lai, L. Lu, and X. Zeng, *Funct. Mater. Lett.* 2, 1250028 (**2012**).
4. K. C. Chan, H. Peng, G. Liu. K. Mcllwrath, F. X. Zhang, R. A. Huggins, and Y. Cui, *Nanotechnol.* 3, 31 (**2008**).
5. Y. S. Chung, J. T. Bloking, and Y. M. Chiang, *Nat. Mater.* 1, 123 (**2002**).
6. M. S. Whittingham, *Chem. Rev.* 104, 4271 (**2004**).
7. F. Croce, G. B. Appetecchi, L. Persi, and B. Scrosati, *Nature* 394, 456 (**1998**).
8. J. K. Feng, H. Xia, M. O. Lai, and L. Lu, *Mate. Res. Bull.* 16, 424 (**2011**).
9. J. Ni, J. Jin, J. P. Wei, Z. Zhou, and J. Yan, *Electrochimica Acta* 17, 349 (**2012**).
10. P. Poizot, S. Laruelle, S. Grugeon, L. Dupont, and J. Tarascon, *M. Nature* 407, 496 (**2000**).
11. F. Badway, I. Plitz, S. Grugeon, S. Laruelle, M. Dolle, A. S. Gozdz, and J. M. Tarascon, *Electrochem. Solid State Lett*. 5, A115 (**2002**).
12. K. T. Nam, D. W. Kim, P. J. Yoo, C. Y. Chiang, N. Meethong, P. T. Hammond, Y. M. Chiang, and A. M. Belcher, *Science* 312, 885 (**2006**).
13. C. K. Chan, H. Peng, R. D. Twesten, K. Jarausch, X. F. Zhang, and Y. Cui, *Nano. Lett.* 7, 490 (**2007**).
14. A. C. Dillon, A. H. Mahan, R. Deshpande, P. A. Parilla, K. M. Jones, and S. H. Lee, *Thin Solid Films* 516, 794 (**2008**).
15. V. Subramanian, W. W. Burke, H. Zhu, and B. J. Wei, *Phys. Chem. C* 112, 4550 (**2008**).
16. Y. S. Ding, X. F. Shen, S. Sithambaram, S. Gomez, R. Kumar, V. M. B. Crisostomo, S. L. Suib, and M. Aindow, *Chem. Mater.* 17, 5382 (**2005**).
17. Y. Tanaka, M. Tsuji, and Y. Tamaura, *Phys. Chem. Chem. Phys.* 2, 1473 (**2000**).
18. Y. S. Horn, S. A. Hackney, C. S. Johnsom, and M. M. Thackeray, *J. Electrochem. Soc.* 145, 582 (**1998**).
19. R. N. Reddy and R. G. Reddy, *J. Power Sources* 132, 315 (**2004**).
20. M. Toupin, T. Brousse, and D. B'elanger, *Chem. Mater.* 16, 3184 (**2004**).
21. V. Subramanian, H. Zhu, R. Vajtai, P. M. Ajayan, and B, *J. Phys. Chem. B* 109, 20207 (**2005**).
22. C. Yan and D. Xue, *Funct. Mater. Lett.* 66, 37 (**2008**).
23. M. Sugantha, P. A. Ramakrishnan, A. M. Hermann, C. Warmsingh, and D. S. Ginley, *Int. J. Hydrog. Energy* 28, 597 (**2003**).
24. R. Yang, Z. Wang, L. Dai, and L. Chen, *Mater. Chem. Phys.* 93, 149 (**2005**).
25. X. Liu, S. Fu, and C. Huang, *Powder Technol.* 154, 120 (**2005**).
26. D. Zheng, S. Sun, W. Fan, H. Yu, C. Fan, G. Cao, Z. Yin, and X. Song, *J. Phys. Chem. B* 109, 16439 (**2005**).
27. Y. Xiong, Y. Xie, Z. Li, and C. Wu, *Chem. Eur. J.* 9, 1645 (**2003**).
28. F. Cheng, J. Chen, X. Gou, and P. Shen, *Adv. Mater.* 17, 2753 (**2005**).
29. E. Machefaux, A. Verbaere, and D. Guyomard, *J. Phys. Chem. Solids* 67, 1315 (**2006**).
30. F. A. Al-Sagheer and M. I. Zaki, *Colloids Surf. A* 173, 193 (**2000**).
31. Z. Yuan, Z. Zhang, G. Du, T. Ren, and B. Su, *Chem. Phys. Lett.* 378, 349 (**2003**).
32. M. Wei, Y. Konishi, H. Zhou, H. Sugihara, and H. Arakawa, *Nanotechnology* 16, 245 (**2005**).
33. Y. L. Ding, J. Xie, G. S. Cao, T. J. Zhu, and H. M. Yu, *J. Phys. Chem. C* 16, 9821 (**2011**).
34. J. E. Post, *Proc. Natl. Acad. Sci. U.S.A.* 96, 3447 (**1999**).
35. D. Portehault, S. Cassaignon, N. Nassif, E. Baudrin, and J. P. Jolivet, *Angew. Chem., Int. Ed.* 47, 6441 (**2008**).
36. Y. Oaki and H. Imai, *Angew. Chem. Int. Ed.* 46, 4951 (**2007**).
37. J. P. Hill, S. Alam, K. Ariga, C. E. Anson, and A. K. Powell, *Chem. Commun*. 383 (**2008**).
38. H. Wang, Z. Lu, D. Quian, Y. Li, and W. Zhang, *Nanotechnology* 18, 115616 (**2007**).
39. X. Chen, L. Jiang, Y. C. Shi, and X. Li, *Solid State Commun.* 136, 94 (**2005**).
40. U. Polona, G. Alexandre, P. Matej, D. Robert, et al., *J. Phys. Chem. C* 113, 14798 (**2009**).
41. P. Poizot, S. Laruelle, S. Grugeon, L. Dupont, and J. M. Tarascon, *Nature* 407, 496 (**2000**).
42. J. C. Guo, Q. Liu, C. S. Wang, and M. R. Zarcariash, *Adv. Fucnt. Mater.* 22, 803 (**2011**).
43. H. Li, P. Balaya, and J. Maier, *J. Electrochem. Soc.* 151, A1878 (**2004**).
44. M. S. Wu and P. C. Chiang, *J. Phys. Chem. B* 109, 23279 (**2005**).
45. A. L. M. Reddy, M. M. Shaijumon, S. R. Gowda, and P. M. Ajayan, *Nano. Lett.* 9, 1002 (**2009**).
46. M. S. Wu, P. C. J. Chiang, J. T. Lee, and J. C. Lin, *J. Phys. Chem. B* 109, 23279 (**2005**).

Received: 29 September 2013. Accepted: 15 January 2014.